Iraqi Journal of Scientific and Industrial Research
Volume 2, Issue (4), October-December 2023, pp. 75-82

Laser-Based Non-equilibrium Low-Temperature Plasma Assisted Combustion Kinetics

Imad BIN SELIMA, Ali EL-MAHDI

Department of Physics, School of Science, Benzert University, Benzert, TUNISIA

Abstract

In this article, advanced laser diagnostics have been used in combination with modeling to study fundamental. We also discuss recent advances in ultra-high frame rate imaging, which provides new capability for capturing the dynamic evolution of high speed, unsteady flow fields, and/or increasing the data collection rate in short run time "impulse" facilities.

Keywords: Thermal equilibrium, Optical measurements, Plasma dynamics, Raman spectroscopy

Received: 19 January 2023; **Revised:** 01 May 2023; **Accepted:** 08 May 2023; **Published:** 1 October 2023

1. Introduction

Thermal disequilibrium among the internal modes of molecular species in supersonic and hypersonic air flows, and in non-equilibrium air, and oxygen containing plasmas, is a widely occurring, but far from well understood, phenomenon which is important to a wide variety of aerodynamic and aerospace platforms. For example, energy storage in vibrational and low lying electronic states of the most common air species (N_2, O_2, NO), including the metastable states O_2 ($a^1\Delta_g$) and N_2 ($A\ ^3\sum^+_u$), are known to have significant, but incompletely understood, influences on the chemistry, shock structure, and heat transfer in the complex flow field around hypervelocity vehicles. The acceleration of low temperature oxidation kinetics by super-equilibrium concentrations of key radical species, such as O, H, OH, etc., produced in high pressure non-equilibrium discharges is similarly recognized but not well understood. In this lecture, an overview of laser diagnostic methods used to probe and characterize such environments will be presented, focusing on recent measurements in N_2, air, and other oxygen containing, nonequilibrium plasmas and high speed flows. The lecture will be divided into three parts. An illustrative survey of laser diagnostic methods which have been successfully employed in measurements of rotational/translational temperature, vibrational distribution function, electronic meta-stable state concentrations, and positive ion and free electron number density. This survey, while by no means complete, is meant to provide the reader with an overview of the power of modern optical diagnostic methodologies and technologies, as well as to provide some guidance on the matching of diagnostic methods with measurement goals. In this paper, it is assumed that the reader has some familiarity with the spectroscopic fundamentals of atoms and diatomic molecules in the gas phase which serve as the foundation for each of the diagnostic measurements discussed, although some specific information relevant to the spectroscopic diagnostics of non-equilibrium systems will be provided. If necessary, more details on the spectroscopic fundamentals of modern laser diagnostics can be found in [1-5]. We will present a more detailed discussion of a recent study in which advanced laser diagnostics have been used in combination with modeling to study fundamental non-equilibrium low temperature Plasma Assisted Combustion kinetics. We also will discuss recent advances in ultra-high frame rate imaging, which provides new capability for capturing the dynamic evolution of high speed, unsteady flow fields, and/or increasing the data collection rate in short run time "impulse" facilities.

Knowledge of the translational energy distribution, which in most cases will be in thermodynamic equilibrium with the rotational energy distribution, is a basic starting point for the characterization and study of non-equilibrium flows and plasmas. The determination of translational temperature is most often based on resolution of the absorption/fluorescence spectral line shape, the very basics of which we present below [1-5]. Very basically, the single photon allowed absorption of electromagnetic radiation is based on Beer's Law

$$\frac{I_t(\upsilon)}{I_o(\upsilon)} = \exp\left(-\kappa_\nu(\nu)L\right) \quad (1)$$

where $I_t(\nu)/I_o(\nu)$ is the ratio of the transmitted intensity, at the frequency ν, to the incident, L is the path length of the radiation through the absorbing medium, and $\kappa_\nu(\nu)$ is the absorption coefficient (with units m^{-1}) at the frequency ν, which is given by

$$\kappa_\nu(\nu) = \left[\frac{nB_{12}N_1h\nu_o}{c}\right]g(\nu-\nu_o) \quad (2)$$

In Eq. (2), B_{12} is the Einstein B coefficient for stimulated absorption, N_1 is the number density of absorbers in the lower quantum state (rotational, vibrational, and electronic) of the absorbing transition, and $g(\nu-\nu_o)$ is the spectral lineshape function. The relationship between the absorption coefficient, $\kappa_\nu(\nu)$, to what is known as the integrated absorption coefficient, is given by

$$\kappa_\nu(\nu) = \left[\int \kappa_\nu(\nu)\right]g(\nu-\nu_o) \quad (3)$$

Note that the units of the integrated absorption coefficient, $\int\kappa_\nu(\nu)$, and spectral lineshape function are $m^{-1}.s^{-1}$, and $1/s^{-1}=Hz^{-1}$, respectively. At low static pressure conditions, on the order of a few torr or less, the spectral lineshape function is well approximated by the well known Doppler profile, given by

$$I(\upsilon) = \frac{1}{\Delta\upsilon_{D,HWHM}}\left[\frac{\ln 2}{\pi}\right]^{1/2} I_o \exp\left[-\frac{\ln 2(\upsilon-\upsilon_o)^2}{\Delta\upsilon^2_{D,HWHM}}\right] \quad (4)$$

where $\Delta\nu_D$ is the Doppler profile Half Width at Half Maximum, which is given by

$$\Delta\upsilon_{D,HWHM} \equiv \left(\frac{\upsilon_o}{c}\right)\sqrt{\frac{(2\ln 2)k_BT}{m}} \quad (5)$$

where k_B is the Boltzmann's coefficient, T is the static temperature of the absorbing medium, and m is the mass of the absorbing atom or molecule

The temperature-dependence of $\Delta\nu_D$ forms the basis of the translational temperature measurement. The Gaussian behavior of the Doppler lineshape function is a direct result of the Maxwellian distribution for atomic/molecular speed, which couples to the wave equation for propagation of electromagnetic radiation via

$$E(t) = E_o\exp\left[-i(\omega_s t + \tilde{k}\bullet\tilde{r}(t)\right] \quad (6a)$$

$$\tilde{r}(t) = \tilde{v}_s t \Rightarrow \quad (6b)$$

$$E(t) = E_o\exp\left[-i(\omega_s t + \tilde{k}\bullet\tilde{v}_s t\right] \quad (6c)$$

$$E(t) = E_o\exp\left[-i(\omega_s + \omega_{Dop})t\right] \quad (6d)$$

where

$$\omega_{Dop} \equiv \tilde{k}\bullet\tilde{v}_s \quad (7)$$

and the wave vector k is given by $k=2\pi n/\lambda$, where n is the medium index of refraction and λ is the radiation wavelength.

Note, for simplicity, a constant amplitude (plane) wave is assumed. In Eq. (6), for the case of simple atomic/molecular absorption, E(t) can be thought of, somewhat simplistically, as the electric field "seen" by the absorbing atom or molecule which is translating through the trajectory r(t). Note that Eq. (6b) requires that the atom or molecule translates at constant vector velocity, **v,** for a total displacement of many times the radiation wavelength. If this is the case then the absorbing frequency is shifted by the quantity ω_{DOP}, and the Maxwellian distribution of atomic/molecular speed gives rise directly to the Gaussian lineshape function, Eq. (5).

Note that while the discussion above refers to simple absorption (or fluorescence) only, a more general treatment of laser scattering (Rayleigh and Raman) is given in Ref. [6]. Finally, note that when the atomic/molecular mean free path between collision is not much greater than the radiation wavelength, then a phenomenon known as "Dicke Narrowing" occurs [7]. A full discussion of this is beyond the scope of this lecture, but more detail on this and the similar phenomenal of rotational narrowing can be found in references [4, 8-11].

At higher pressures, in particular when the collision mean free path is much less than the radiation wavelength, the Doppler lineshape function is replaced by the Lorentzian "collisional" (also known as pressure) broadening lineshape given by

$$I(w) = \frac{I_o}{\pi}\left[\frac{\gamma_{coll}}{\left[(\omega-\omega_o)^2+\gamma^2_{coll}\right]}\right] \quad (8)$$

where γ_{coll} is the collisional broadening coefficient. Note that with the Lorentz function as defined in Eq. (8), γ_{coll} corresponds to the spectral Half Width at Half Maximum. In general, γ_{oll} is determined experimentally and given by an expression of the form

$$\gamma_{coll} = P\Delta\upsilon_{coll}(T) = P\Delta\upsilon_{coll,298}\left(\frac{298K}{T}\right)^x \quad (9)$$

For what is known as the hard sphere collision model, the exponent x is equal to 0.5, from simple kinetic theory. For most realistic inter-molecular potentials, the exponent x is in the range 0.5–1.0, with a value of approximately 0.7 being not uncommon.

At intermediate pressures (typically in the approximate range 0.05-0.5 bar for visible wavelengths), where neither Doppler nor pressure broadening predominate, the lineshape can in most cases be well approximated by a convolution of Eq. (4) and (8) known as the Voigt scattering profile, given by

$$I(\upsilon)=\left(\frac{\gamma_L}{\gamma_D}\right)\left(\frac{1}{\pi}\right)\left(\frac{\ln 2}{\pi}\right)^{1/2}\int_{-\infty}^{\infty}\left[\frac{d\upsilon'}{(\upsilon-\upsilon_o-\upsilon')^2+\gamma_L{}^2}\right]\exp\left[-(\ln 2)\frac{(\upsilon'-\upsilon_0)^2}{\gamma_D^2}\right] \quad (10)$$

where, again, the line broadening coefficients are defined as Half Width at Half Maximum. Following the notation of Laufer [5], the Voigt profile can be written in more compact form as

$$I(\upsilon)=\left(\frac{B}{\pi\gamma_D}\right)\left(\frac{\ln 2}{\pi}\right)^{1/2}\int_{-\infty}^{\infty}\left[\frac{e^{-y^2}}{(D-y)^2+B^2}\right]dy \quad (11)$$

where

$$y\equiv(\ln 2)^{1/2}\left(\frac{\upsilon'}{\gamma_D}\right), \qquad B\equiv(\ln 2)^{1/2}\left(\frac{\gamma_L}{\gamma_D}\right),$$

$$D\equiv(\ln 2)^{1/2}\left(\frac{\upsilon-\upsilon_o}{\gamma_D}\right)$$

An example of the use of the Voigt profile will be presented below.

The determination of rotational temperature is based on simple statistical mechanics, specifically the use of the Boltzmann distribution for rotational energy [12]

$$f_J=\frac{(2J*1)\exp\left[\frac{-E_J}{k_BT}\right]}{q_{rot}(T)} \quad (13)$$

where $q_{rot}(T)$ is the rotational partition function and E_J is the energy of the J^{th} rotational quantum level, which for a rigid rotor wave function is given by $E_J=B(J)(J+1)$ where B is a constant

At room temperature, for simple diatomic molecules like O_2 and N_2, B, in cm^{-1} units is approximately two. Numerous diagnostic methods which utilize the rotational Boltzmann distribution for determination of temperature exist in the literature, including, to name only a few, the use of diode laser absorption spectroscopy [13], two (or more) line Laser Induced Fluorescence [14], pure rotational Raman spectroscopy [15], and coherent Anti-Stokes Raman spectroscopy (CARS) [16]. Examples of the latter two methods will be presented below.

As a recent example of determination of translational/rotational temperature we cite the measurements of Parker et al. [17] who have performed tunable diode laser absorption spectroscopy (TDLAS) in the LENS 1 hypersonic facility. TDLAS has experienced enormous growth in recent years due to the robustness and relative low cost of the instrumentation, and the inherently quantitative feature of absorption spectroscopy. In particular, the technique has been used widely in combustion and sensor systems, a thorough recent review of which has been given by Allen et al. [13]. LENS 1 is a hypersonic shock tunnel in which a driver/test gas is compressed to static temperatures as high as 8000 K, and then expanded in an isentropic nozzle to velocities as high as ~4.2 km/s [18]. The steady test time is on the order of several millisecond. The LENS diode laser work uses naturally abundant NO, formed in the plenum of the hypersonic shock tunnel, as the absorbing molecule. As discussed in [17], non-equilibrium kinetic modeling had predicted NO mole fraction in the free stream LENS 1 flow as high as ~6%. The purpose of these studies was to quantify the actual NO concentration produced, as well as to serve as validation measurements for the computational predictions. Figures (1) and (2) show two typical single spectral trace diode laser absorption measurements, taken at 5 MJ/kg and 10 MJ/kg tunnel enthalpy conditions, respectively. Note that in both cases the data traces were obtained on a time scale of approximately 1 ms (1 kHz diode laser sweep rate). The two spectral absorption features coincide to a single, rotational transition within the fundamental vibrational band of the ground electronic state of NO, which exhibits a phenomenon known as lambda doubling [19]. Note that the lambda doubling fine structure splitting, ~0.01 cm^{-1}, is essentially completely resolved, a demonstration of the inherently high spectral resolution of the TDLAS approach.

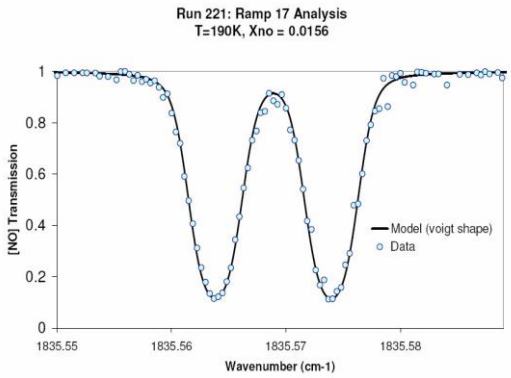

Fig. (1) Single Trace TDLAS spectrum obtained in LENS 1 facility at 5 MJ/kg enthalpy

The fits to the data utilize the Voigt profile, Eq. (10), with the known free steam temperature and pressure as input data to a spectral modeling code based on the well known HITRAN data base [20]. Referring to Eq. (2), the HITRAN data base returns the equivalent of the value for the Einstein B coefficient, including rotational line strength factors, and values for the collisional (Lorentz) broadening coefficient at the free stream temperature. The free stream temperature is also used to determine the

rotational Boltzmann fraction for the chosen transition, which along with the ideal gas equation gives the value for N_1 in Eq. (2).

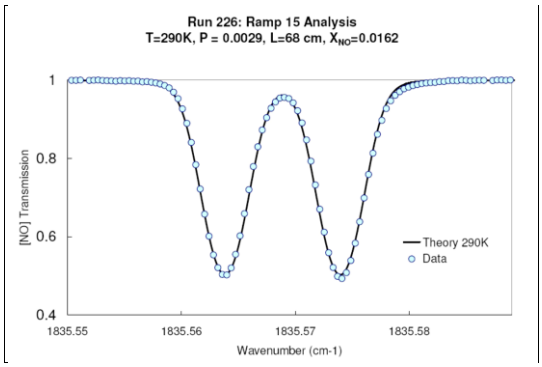

Fig. (2) Single Trace TDLAS spectrum obtained in LENS 1 facility at 10 MJ/kg enthalpy

For the 5 MJ/kg case (Fig 1), the temperature and NO mole fraction inferred from the best fit to the spectral model are 190 K and 0.0156, respectively. While the inferred temperature is in reasonable agreement with that calculated from non-equilibrium CFD codes, 229 K, the experimentally determined NO mole fraction is factor of approximately three less than the ~5% predicted from the calculations. For the 10 MJ/kg case (Fig. 2), the experimentally inferred temperature and NO number density were 290 K and 0.016, respectively, as compared to CFD predictions of 563 K and 0.054. These discrepancies are a subject of on-going research.

Finally, it should also be noted that for the 5 MJ/kg condition the authors were able to make a novel measurement of rotational temperature, based on the known relative isotopic abundances of $^{14}N^{16}O$, the primary isotopomer, and $^{14}N^{18}O$ and $^{15}N^{16}O$. Each of these species exhibited a detectable absorption feature within the scanning range of the diode laser. Since the specific absorptions for each isotopomer corresponded to different values of rotational quantum number, the rotational temperature could be determined from the known isotopic abundances. The resulting value was 190 K, in excellent agreement with that inferred from the Voigt profile determination.

As a second example, we cite the recent pure rotational Raman temperature measurements obtained in a laser pumped non-equilibrium oxygen containing plasma by Frederickson, et al. [21]. Raman scattering is a relatively simple optical diagnostic capable of quantitative determination of heavy species rotational/translational temperature, and vibrational distribution function of major species. Very basically (more detail can be found in [22-23]), scattering can be explained, classically, as the result of an incident electromagnetic wave inducing an oscillating electric dipole moment, p(t) which is given by the product of the polarizability, α, of the medium and the time-varying incident electric field ,E(t).

$$p(t) = \alpha \cdot E(t) \tag{14}$$

The polarizability is customarily expanded with respect to the vibrational normal coordinates (or "normal modes"), Q, of the molecule as

$$\alpha = \alpha_0 + \left(\frac{\partial \alpha}{\partial Q}\right)_0 Q + \cdots \tag{15}$$

where α_0 and $(\partial\alpha/\partial Q)_0$ are evaluated at the equilibrium internuclear displacement. Assuming harmonic oscillation of a single vibrational mode with natural frequency ω_k, so that $Q = Q_0 \cos(\omega_k t)$, and sinusoidal applied electric field, E, with frequency ω_l and amplitude E_o, the induced electric dipole moment is given by

$$p(t) = \left[\alpha_0 + \left(\frac{\partial \alpha}{\partial Q}\right)_0 Q_0 \cos(\omega_k t)\right] E_0 \cos(\omega_1 t) = \alpha_0 E_0 \cos(\omega_1 t) + \left(\frac{\partial \alpha}{\partial Q}\right)_0 \frac{Q_0 E_0}{2}\left[\cos(\omega_1 - \omega_k)t + \cos(\omega_1 + \omega_k)t\right] \tag{16}$$

The first term in Eq. (16) contributes to Rayleigh (and Thomson) scattering, and to pure rotational Raman scattering, an example of which will be given directly below. The second term represents vibrational Raman scattering.

In recent years, Rayleigh/Raman scattering has been augmented by the use of atomic/molecular vapor filters as narrow bandwidth filters and/or as spectral discriminators. The basic idea, illustrated in Fig. (3), is to utilize a narrow spectral line width laser which is tuned to a strong absorption resonance of the vapor.

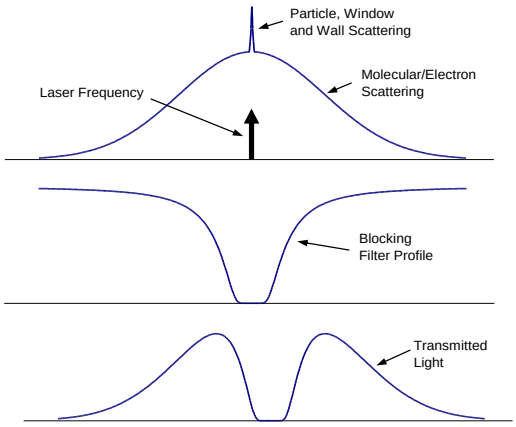

Fig. (3) Basic Filtered Rayleigh Scatting concept

If a cell filled with the vapor is then inserted into the path between the scattering volume and the detector, elastic scattering can be attenuated while Doppler shifted and/or broadened scattering can be transmitted. In fact, the use of such vapor filters for Raman scattering dates to near the discovery of the Raman effect itself [25], although it is only with recent advances in laser technology that their true utility has been realized. In addition to continuous wave (cw) Raman instruments incorporating mercury vapor [26] and rubidium vapor [27,28], the availability of high power, narrow spectral line width pulsed laser sources as common laboratory tools has enabled a wide range of new vapor filter-based scattering techniques. Most of these have utilized iodine vapor, which is particularly convenient because of strong absorption resonances within the tuning range of injection-seeded, pulsed Nd:YAG lasers, as well as the relative ease of filter construction, and availability of high quantum efficiency detectors, both for point measurements and for imaging. A variety of molecular filter-based diagnostics, including velocity imaging, in which Doppler shifted Rayleigh or Mie scattering is converted to velocity by determination of the fractional transmission through a vapor filter, and temperature imaging, which is similar to velocity imaging but is based on Doppler broadening of molecular Rayleigh scattering, as opposed to Doppler shift, was presented [29]. Other examples include: High Spectral Resolution Light Detection and Ranging (HSRL) [30] and, most recently, Thomson [29,31] and pure rotational Raman scattering [15], examples of both of which will be given in these notes.

Figure (4) shows a filtered pure rotational Raman spectrum of N_2 at 500 torr and room temperature, using a pulsed Ti:sapphire laser – rubidium filter combination described by Lee and Lempert [15,24]. As described in [15,24], the effect of the filter was to reduce the intensity from stray light and molecular Rayleigh scattering by a factor as high as ~10^6, while transmitting greater than 80% of the rotational Raman scattering.

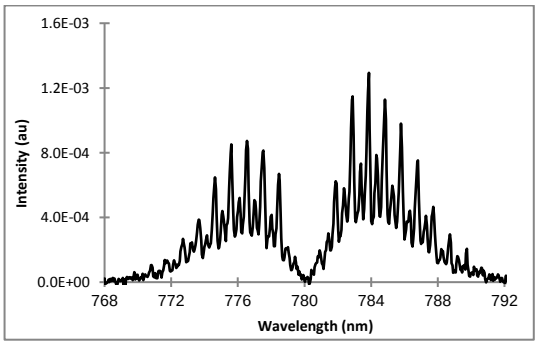

Fig. (4) Pure rotational Raman spectrum of N_2 obtained with a rubidium vapor filter

Filtered pure rotational Raman spectra, similar to that shown in Fig. (4), have been used by Frederickson et al [21], and Lee et al. [32] as part of a study of the influence of vibrational excitation on the low temperature rate of the three body free electron attachment to O_2 process

$$O_2 + e^- + M \leftrightarrow O_2^- + M \quad (17)$$

These studies utilized the apparatus shown in Fig. (5a). A continuous wave CO laser creates a highly vibrationally non-equilibrium synthetic CO-seeded air mixture at ~1 bar pressure and room temperature, using a process known as Anharmonic V-V transfer [33]. The vibrational distribution functions (VDF) of all three components CO, O_2, and N_2, are determined from vibrational Raman scattering using an Nd:YAG laser (not shown in Fig. 5). Rotational temperature is determined using a line narrowed titanium:sapphire laser, which is input collinearly to the CO laser, and can be translated radially with respect to the CO laser beam centerline in order to provide radially resolved temperature data. A pulsed electron beam is input to the non-equilibrium air mixture through a foil window, and time-dependent electron density measured using a simple microwave attenuation apparatus.

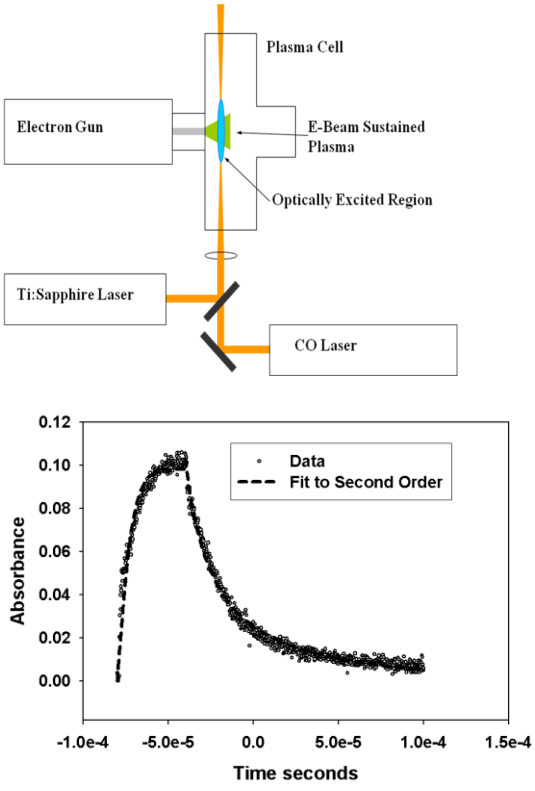

Fig. (5) Apparatus (upper) and typical time dependent electron density trace (lower) from O_2 free electron attachment mitigation studies of Frederickson

Figure (5b) shows typical results for rise and fall of the electron density for a 10 μs duration square primary electron beam current pulse. While not shown, when the CO excitation laser is not present, the electron density trace replicates precisely the 10 μs square e-beam pulse with no hint of the long,

exponential decay (or rise) evident in Fig. (5b). From simple modeling, including both O_2 attachment, Eq. (17), and electron-ion recombination, which becomes the dominant process in the vibrationally excited medium, it is determined that the experimentally observed increase in the pulsed plasma lifetime is due to a five order or magnitude increase in the backwards, detachment rate of process (17), which results from vibrational excitation of M, the third body collision partner.

While the raw electron density data clearly showed complete mitigation of electron attachment, it was not clear whether this was truly a non-equilibrium effect, due to vibrational excitation, or a thermal effect, due to the known rapid increase in the reverse (detachment) rate of process (17) with increasing temperature. Figure (6) shows a filtered pure rotational Raman spectrum (S-branch only) obtained *in-situ* in the apparatus shown in Fig. (5a), in the presence of the CO excitation laser, along with a least squares fit. The resulting rotational temperature is 350±7K, ~300K lower than that required to produce the long plasma lifetime observed in Fig. (5b), had the effect been thermal.

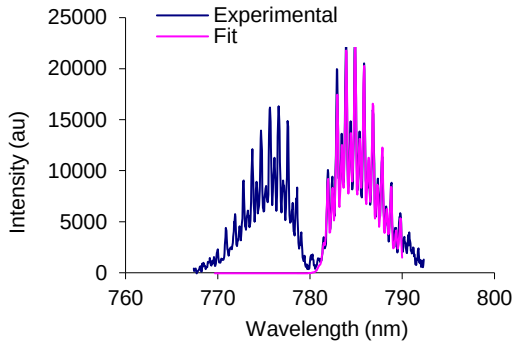

Fig. (6) Filtered pure rotational Raman spectrum of optically pumped N_2/CO mixture at 1 bar pressure and least squares spectral fit. Inferred temperature is 355±7K

As a final example of T-R (translational/rotational) temperature measurements in plasmas, the recently developed coherent Rayleigh scattering diagnostic is cited [34,35]. As illustrated on the left hand side of Fig. (7), coherent Rayleigh is a non-linear four wave mixing process, similar to coherent anti-Stokes Raman spectroscopy (CARS), in which a pair of "pump" beams are overlapped in a fluid to form a traveling wave "grating" pattern similar to that from ordinary Laser Doppler Velocimetry. In this case, the grating results from electrostriction, in which the traveling wave regions of high and low electric field induce a traveling wave density perturbation in the fluid. In essence, extra molecules are trapped in the traveling wave potential well caused by the interference pattern from the two pump beams. If the amplitude of the potential well is not too large (i.e., the laser beam intensities are not too high) than the molecules which become trapped are those which are already traveling with velocity near that of the grating. In other words, for weak fields, the pump laser beams do not greatly perturb the velocity distribution of the probed fluid. In its simplest configuration, scanning the frequency of one pump beam relative to the other causes the traveling wave velocity to be scanned.

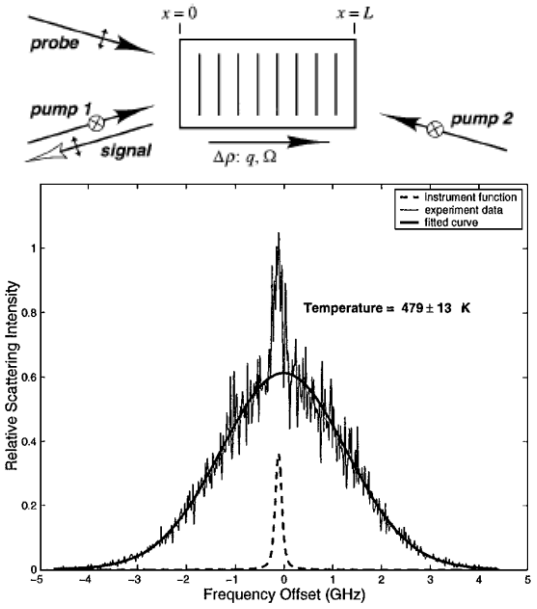

Fig. (7) Schematic illustration of coherent Rayleigh scattering, and example spectrum from argon glow discharge plasma at 50 mbar

The relative scattering efficiency of the probe beam, as the traveling wave velocity is scanned, constitutes a measurement of the relative distribution of molecular velocity of the probed fluid molecules, i.e., the translational temperature. An example coherent Rayleigh spectrum, obtained from an argon glow discharge plasma at 50 mbar [35], is shown on the right side of Fig. (7). The inferred temperature is 479±13K. Note that this spectrum was obtained using a broad band pump beam, enabling "single shot" capability similar to that routinely employed for CARS. The spectrum was resolved using a Fabry-Perot etalon.

Determination of the vibrational distribution function (VDF) is a central measurement requirement in non-equilibrium air flows and plasmas. In general, there are four common mechanisms by which the vibrational mode of constituent molecular species can be overpopulated. The first mechanism is the well-known freezing of the thermal population formed in a high temperature plenum upon rapid supersonic/hypersonic expansion [36]. The second is due to quenching of electronically excited states, which can lead to highly vibrationally excited distributions in the ground electronic state. For example N_2 (A) state quenching, and the influence of this process on NO production in air plasmas. The third is the inherent non-equilibrium formed by resonant absorption of radiation, such as that from a CO laser [37].

Similar to resonant absorption, the fourth common mechanism of vibrational excitation is that due to electron impact excitation in plasmas and discharges which operate with an intermediate value of what is known as the reduced electric field, *E/n*. Briefly, more detail can be found in [38], the reduced electric field of a weakly ionized atomic/molecular plasma is a measure of the average kinetic energy to which a free electron in the plasma is accelerated in the interval between inelastic collisions with heavy species (A similar definition holds for fully ionized plasmas, but in this case the n refers to electron density).

In general, the plasma *E/n* value correlates with the average electron temperature and electron energy distribution function (EEDF). Figure (8) illustrates this for air plasmas. Note that a common unit for reduced electric field is the Townsend, Td, which is defined at 10^{-17} V-cm^2. Typical weakly ionized diffuse "glow" discharges operate in the *E/n* range between approximately 10 and 100 Td. It can be seen, for example, that at an *E/n* value of ~100 Td, approximately half the energy deposited into the discharge results in electron impact excitation of the N_2 vibrational mode.

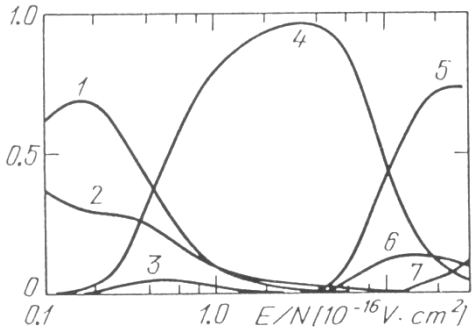

Fig. (8) Typical distribution of energy in air discharges between internal modes as a function of *E/n* [1: O_2 vibration, 2: Rotation, 3: Elastic Losses, 4: N_2 vibration, 5: N_2 electronic states, 6: O2 electronic states, 7: Ionization]

References

[1] Eckbreth A.C., **"Laser Diagnostics for Combustion Temperature and Species"**, 2nd ed., Gordon and Breach Publishers, Amsterdam, 1996.
[2] Linne M. A., **"Spectroscopic Measurement – An Introduction to the Fundamentals,"** Academic Press, Amsterdam, 2002.
[3] Kohse-Hoinghaus K. and Jeffries J.B., **"Applied Combustion Diagnostics,"** Taylor and Francis, New York, 2002.
[4] Demtroder W., **"Laser Spectroscopy – Basic Concepts and Instrumentation,"** Springer, Berlin, 2nd ed., 1996.
[5] Laufer G., **"Introduction to Optics and Lasers in Engineering,"** Cambridge University Press, Cambridge, 1996.
[6] Lempert W., in *Non-Equilibrium Air Plasmas at Atmospheric Pressure*, edited by Becker, K., Kogelschatz, U., Schoenbach, K.H., and Barker, R., IOP Publishing, Bristol, UK, 2005, Ch. 8, "Diagnostics."
[7] Dicke R.H., *Phys. Rev.*, 89 (1953) 472.
[8] Bonamy L. et al., *J. Chem. Phys.*, 89 (1988) 5568.
[9] Rosasco G.J. et al., in "Spectral Line Shapes, Vol. 2, Walter de Gruyter & Co., Berlin, p. 635 (1983).
[10] Galatry L., *Phys. Rev.*, 122 (1961) 1281.
[11] Hall R.J., Verdieck J.F. and Eckbreth A.C., *Opt. Commun.*, 35 (1979) 69.
[12] McQuarrie D.A. and J.D Simon, **"Physical Chemistry – A Molecular Approach,"** University Science Books, Sausilito CA, 1997.
[13] Allen M.G., E.R. Furlong and R.K. Hanson, "Tunable Diode Laser Sensing and Combustion Control," in *"Applied Combustion Diagnostics,"* edited by K. Kohse-Hoinghaus and J. B. Jeffries, Taylor and Francis, New York, 2002.
[14] McMillan B.K., J.L. Palmer and R.K. Hanson, *Appl. Opt.*, 32 (1993) 7532- 7545.
[15] Lee W. and W.R. Lempert, *AIAA Journal*, 40(12) (2002) 2504–2510.
[16] Harvey A.B., **"Chemical Applications of Nonlinear Raman Spectroscopy,"** Academic Press, New York, 1981.
[17] Parker R.A. et al., AIAA-2006-926, 44th AIAA Aerospace Sciences Meeting, Reno, NV, 9-12 January, 2002.
[18] Holden M. and R.A. Parker, "Lens Hypervelocity Tunnels and Application to Vehicle Testing at Duplicated Flight Conditions," Ch. 4, Advanced Hypersonic Test Facilities, Editors F. Lu and D. Marren, Vol. 198, 2002.
[19] Herzberg G., "Molecular Spectra and Molecular Structure – Vol. I Spectra of Diatomic Molecules," Krieger Publishing Company, Malibar, FL, reprint edition (1989).
[20] Rothman L.S. et al., "The HITRAN molecular spectroscopic database: editor of 2000 including updates through 2001," *JQSRT*, 82 (2003) 5.
[21] Frederickson K. et al., *J. Appl. Phys.*, 101 (2007) 093302.
[22] Long D.A., **"The Raman Effect"**, John Wiley & Sons, London, 2002.
[23] Weber A., **"Raman Spectroscopy of Gases and Liquids,"** Springer-Verlag, Berlin, 1979.
[24] Lee W. and W. Lempert, *Appl. Opt.*, 42 (2003) 4320-4326**.**
[25] Rasetti F., *Nuovo Cimento*, 7 (1930) 261.
[26] Pelletier M.J., *Appl. Spectroscopy*, 46(3) (1992) 395-400.
[27] Indralingan R. et al., *Anal. Chem.*, 64 (1991) 964-967.
[28] Clops R. et al., *Appl. Spectroscopy*, 54(9) (2000) 1391-1398.

[29] Miles R.B. et al., *Measur. Sci. Technol.*, 12(4) (2001) 442-451.
[30] Shimizu H., Lee S.A., and She C.Y., *Appl. Opt.*, 22(9) (1983) 1373-1381.
[31] Bakker L.P. and Kroesen G.M., *J. Appl. Phys.*, 88 (2000) 3899.
[32] Lee W. et al., "Mitigation of Oxygen Attachment in High Pressure Plasmas by Vibrational Excitation, AIAA-2004-2257, 35th AIAA Plasmadynamics and Laser Meeting, Portland, OR, 28 Jun – 01 July, 2004.
[33] Treanor C.E., J.W. Rich and R.G. Rehm, *J. Chem. Phys.*, 48 (1968) 1798-1807.
[34] Grinstead J.H. and P.F. Barker, *Phys. Rev. Lett*. 85 (2000) 1222.
[35] Pan X., *Opt. Lett.*, 27 (2002) 161.
[36] de Roany C. de G. et al., *AIAA Journal*, 31 (1993) 119.
[37] Lee W., Adamovich I.V. and Lempert W.R., *J. Chem. Phys.*, 114(3) (2001) 1178-1186.
[38] Raizer Y.P., **"Gas Discharge Physics"**, Springer-Verlag, Berlin, 1991.

